Electronic Supplementary Material (ESI) for Journal of Materials Chemistry A.

Supplementary Information

Unveiling Ligand-Mediated Phase Engineering Mechanism in Two-Dimensional Transition Metal Chalcogenides through Coordination Geometry Control

Sungju Jun,[1] Joo-Won Lee,[1] Sung-Chul Kim,[2] Soong Ju Oh,[3] and Sohee Jeong*[1]

[1] Materials Architecturing Research Center, Korea Institute of Science and Technology, Seoul, 02792, South Korea

[2] Advanced Analysis and Data Center, Korea Institute of Science and Technology, Seoul, 02792, South Korea

[3] Department of Materials Science and Engineering, Korea University, Seoul 02841, South Korea

Experimental section

Chemical

Tungsten hexacarbonyl ($W(CO)_6$, 97%, Sigma-Aldrich) , trioctylphosphine oxide (TOPO, technical grade, 90%, Sigma-Aldrich), hexadecylamine (HDAm, technical grade, 90%, Sigma-Aldrich), triphenylphosphine oxide (TPPO, 98%, Sigma-Aldrich), selenium (Se, 99.99% trace metals basis, Sigma-Aldrich), sulfur (S, 99.98% trace metal basis, Sigma-Aldrich), toluene (>99.8%, SAMCHUN pure chemical), acetone (99.7%, SAMCHUN pure chemical), and ethanol (99.9%, SAMCHUN pure chemical) were used as received without further purification. Oleylamine (OLAm, technical grade, 70%, Sigma-Aldrich), and 1-octadecene (ODE, technical grade, 90%, Sigma-Aldrich) were used after purification.

Synthesis of 1T'-WSe_2 nanosheets

For the synthesis of 1T'-WSe_2:TOPO, 1.0 mmol of $W(CO)_6$, 1.6 mmol of Se, 20 mmol of TOPO, and 20 mL of ODE were loaded in a 3-neck flask. The mixture was heated up to 330 ^oC for 40 min under Ar protection and kept for 2 h. The reaction pot was quenched using acetone to room temperature. 1T'-WSe_2 nanosheets were collected by centrifugation at 7,000 rpm with acetone and washed several time with toluene and ethanol. Finally, 1T'-WSe_2 nanosheets were dried and stored in glove box. In the case of 1T'-WSe_2:TPPO, the same synthetic procedure was adopted except the introduction of TPPO (20 mmol) for replacing TOPO.

Synthesis of 2H-WSe_2 nanosheets

The synthesis of 2H-WSe_2 nanosheets was conducted via the same process as for 1T'-WSe_2:TOPO except that TOPO was replaced by the ligands (80 mmol of OLAm for 2H:WSe_2:OLAm and 80 mmol of HDAm for 2H:WSe_2:HDAm).

Synthesis of 1T-WS_2 and 2H-WS_2 nanosheets

The synthesis of 1T-WS_2:TOPO and 2H-WS_2:OLAm was performed via the same methods for 1T'-WSe_2:TOPO and 2H-WSe_2:OLAm, respectively, except that Se was replaced by S (1.6 mmol).

Synthesis of W precursor complexes ($W(CO)_6$:OLAm-T and $W(CO)_6$:TOPO-T)

$W(CO)_6$ and OLAm were added to a 3-neck flask with the molar ratio of 1:8. The mixture was heated up to the target temperatures (T = 50, 100, 150, 200 °C). For the synthesis of $W(CO)_6$:TOPO-T, $W(CO)_6$ and TOPO were reacted instead of OLAm at the same temperatures.

Selenization of $W(CO)_6$:OLAm-200 and $W(CO)_6$:TOPO-200

For the selenization process, a Se solution was injected to each flask containing $W(CO)_6$:OLAm-200 and $W(CO)_6$:TOPO-200, respectively, where a Se solution was prepared by dissolving Se powders in ODE under Ar protection. The selenization process was conducted at 330 °C and maintained for from 10 to 60 min.

XANES measurement

W L_1-edge XANES measurements were conducted at the 1D KIST-PAL beamline in Pohang Accelerator Laboratory (PAL). W L_1 pre-edges and rising edges were fitted using the Athena program.

Electrochemical measurement

For preparing catalyst inks, 10 mg of 2H-WSe_2:OLAm and 1T'-WSe_2:TOPO, respectively, 60 μL of Nafion-117, and 1 ml of ethanol were mixed together. Each catalyst ink was dropped onto glassy carbon electrode (GCE) with the 3 mm diameter to be a catalyst loading of 0.65 mg/cm^2. Linear sweep voltammetry was carried out to obtain polarization curves of 2H-WSe_2:OLAm and 1T'-WSe_2:TOPO in a Ar-saturated 0.5 M H_2SO_4 solution with a scan rate of 10 mV/s using a graphite electrode as the counter electrode and a saturated calomel (Hg/$HgCl_2$

in saturated KCl) as the reference electrode. To obtain double-layer capacitances of 2H-WSe_2:OLAm and 1T'-WSe_2:TOPO, cyclic voltammetry measurements were conducted at different scan rates from 20 mV/s to 120 mV/s. The chronopotentiometry result of 1T'-WSe_2:TOPO was collected at the current density of -10 mA/cm^2 for exploring the long-term durability.

Characterization

Atomic arrangements were investigated by transmission electron microscopy (TEM) and high-angle annular dark-field scanning transmission electron microscopy (HAADF-STEM). Powder X-ray diffraction (PXRD) patterns were measured using an Empyrean diffractometer (Malvern Panalytical) equipped with a Cu K-alpha radiation source. Raman spectra were recorded by a confocal Raman microscope (inVia Reflex, Renishaw) with the laser excitation wavelength of 532 nm. X-ray pair distribution function (XPDF) measurements were conducted using a PANalytical Empyrean multipurpose diffractometer equipped with Ag anode (λ = 0.5609 Å), a focusing mirror and a GaliPIX3D detector with CdTe sensor. Fourier transform infrared (FTIR) transmittance were obtained using a Nicolet iS50 FTIR spectrometer (Thermo Fisher Scientific). X-ray photoelectron spectroscopy (XPS) results were obtained using PHI 5000 VersaProbe instrument to investigate the chemical states.

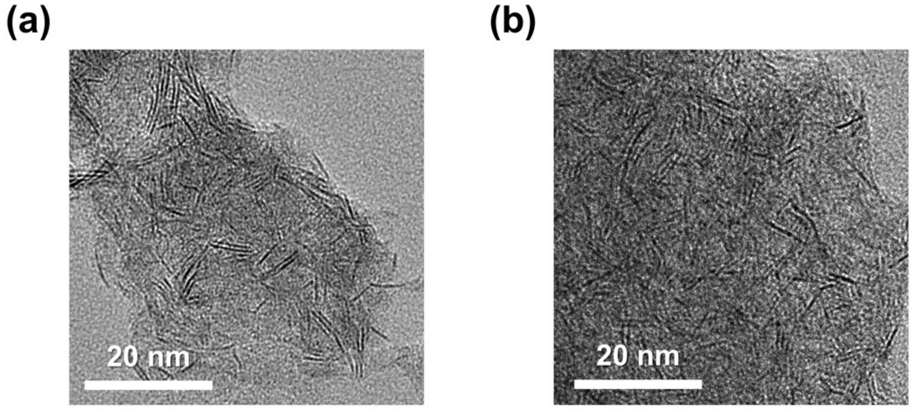

Figure S1. TEM images of (a) 2H-WSe_2:OLAm and (b) 1T'-WSe_2:TOPO.

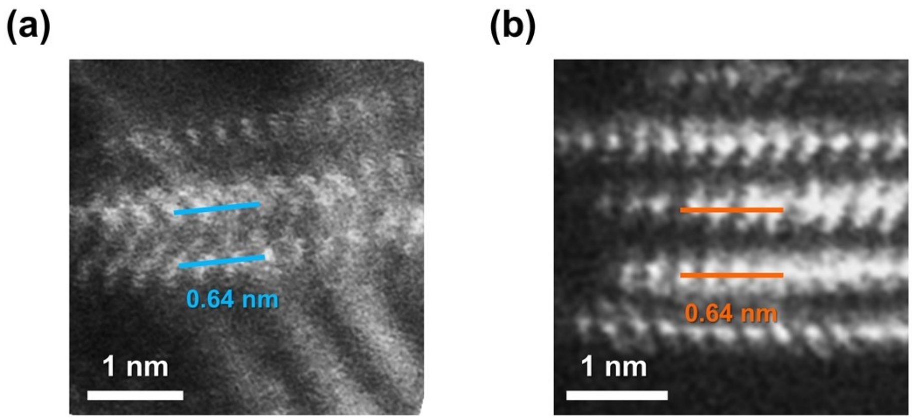

Figure S2. Side-view HAADF-STEM images of (a) 2H-WSe_2:OLAm and (b) 1T'-WSe_2:TOPO, showing their interlayer distances.

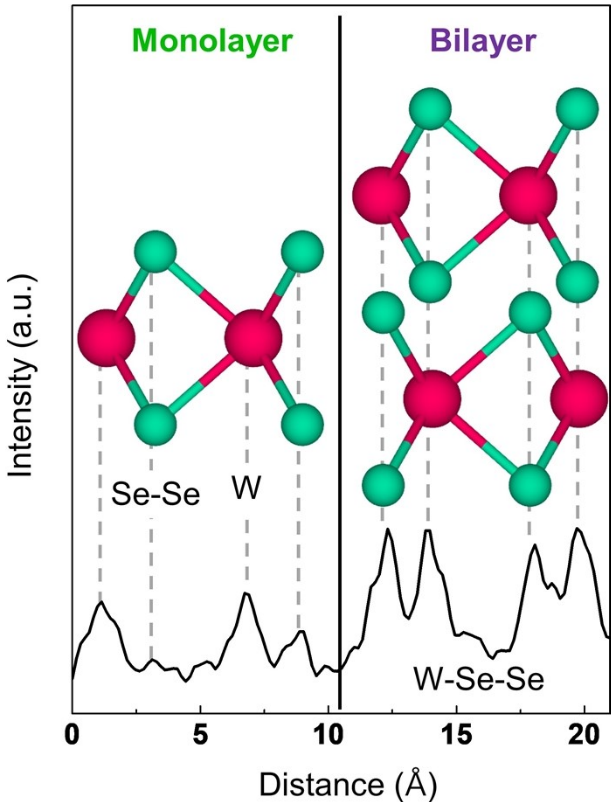

Figure S3. STEM intensity profile along the monolayer and bilayer region of 2H-WSe_2:OLAm in Figure 1b. The intensity profile reflects the atomic sequences of monolayer 2H-WSe_2 (W and Se–Se) and bilayer 2H-WSe_2 (W–Se–Se) along the *c*-direction.

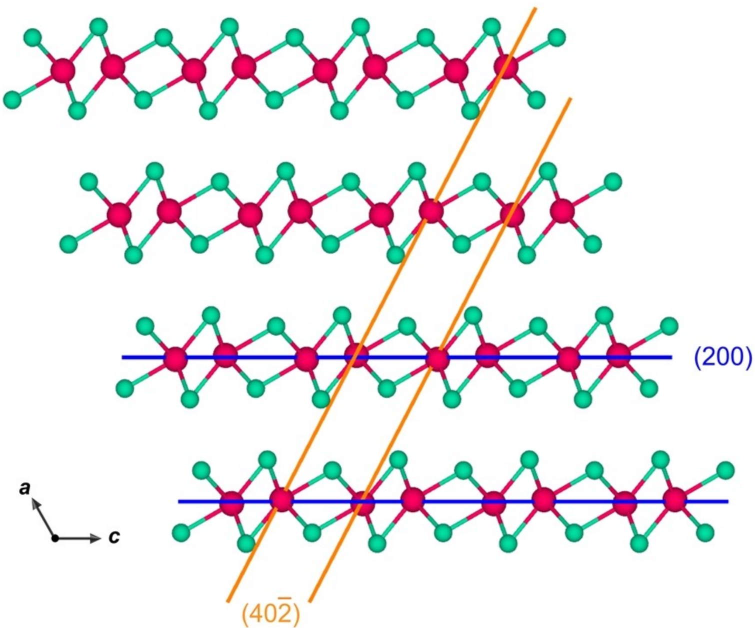

Figure S4. Schematic structure of 1T'-WSe_2 with (200) and (40-2) crystallographic planes highlighted.

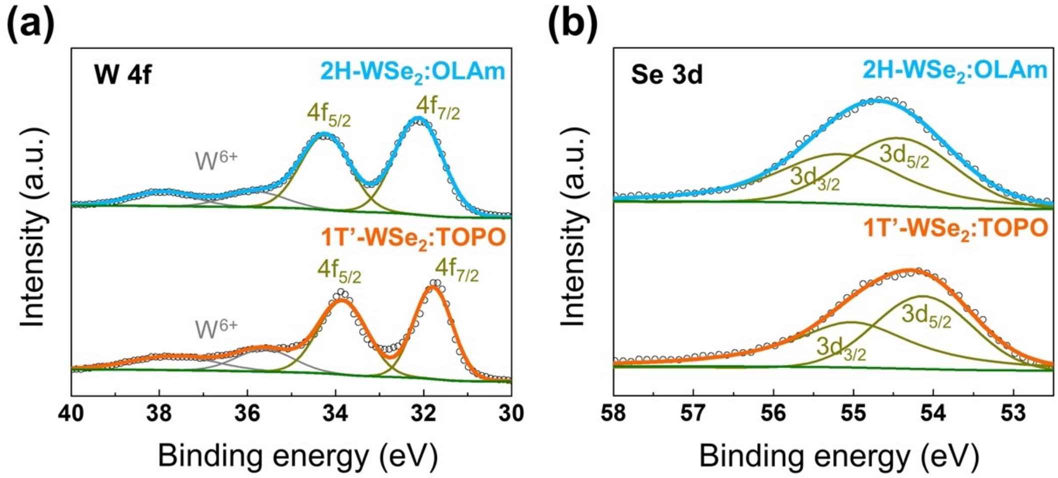

Figure S5. High-resolution XPS spectra of 2H-WSe_2:OLAm and 1T'-WSe_2:TOPO at the core level of (a) W 4f and (b) Se 3d.

Table S1. Calculated atomic-pair distances of 2H-WSe_2 and 1T'-WSe_2.

2H–WSe_2		**1T'–WSe_2**	
Atomic pair	Distance	Atomic pair	Distance
W–Se(1) (nearest pair)	2.526 Å	**W–Se(1)** (nearest pair)	2.493 Å
			2.493 Å
			2.514 Å
			2.583 Å
			2.583 Å
			2.609 Å
W–W	3.282 Å	**W–W_{sh}**	2.777 Å
		W–W_b	3.265 Å
		W–W_{el}	3.979 Å
W–Se(2)	4.141 Å	**W–Se(2)**	3.825 Å
			4.121 Å
			4.180 Å

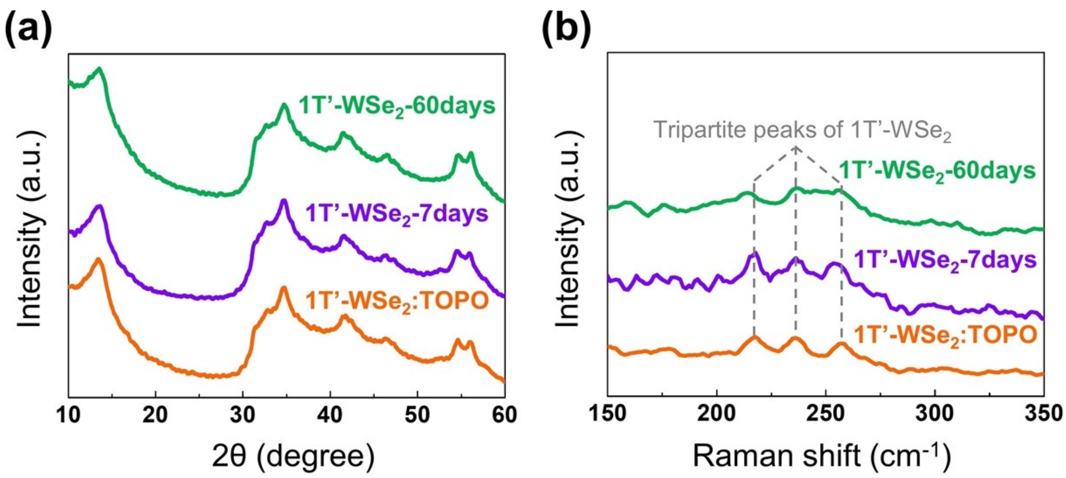

Figure S6. (a) XRD patterns and (b) Raman spectra of freshly prepared 1T'-WSe_2:TOPO and 1T'-WSe_2:TOPO that have been stored in ambient condition for 7 and 60 days (1T'-WSe_2-7days and 1T'-WSe_2-60days, respectively).

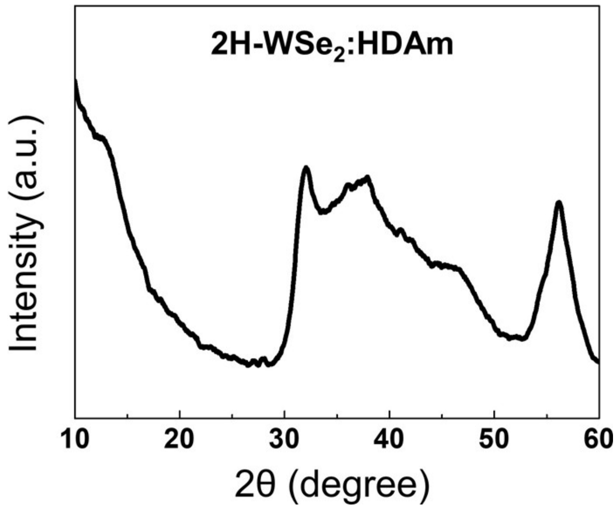

Figure S7. PXRD pattern of 2H-WSe_2 nanosheets grown by hexadecylamine (2H-WSe_2:HDAm).

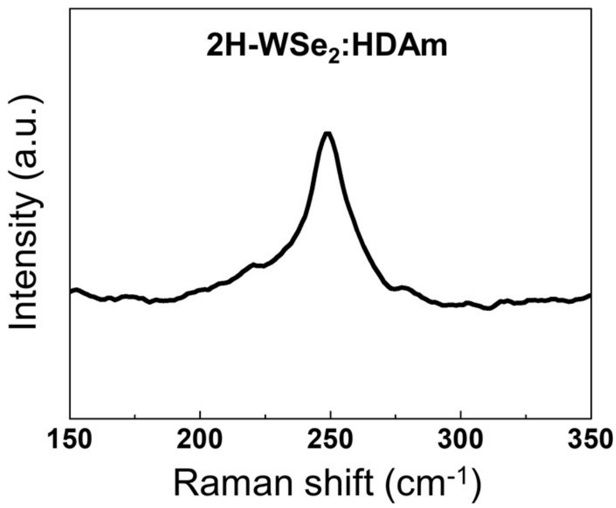

Figure S8. Raman spectrum of 2H-WSe_2:HDAm.

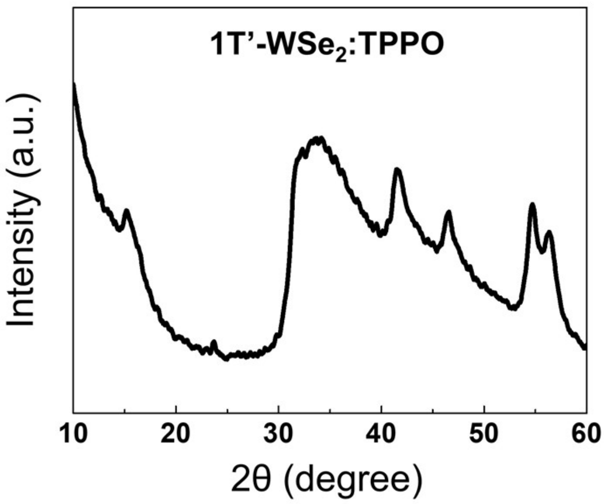

Figure S9. PXRD pattern of 1T'-WSe_2 nanosheets grown by triphenylphosphine oxide (1T'-WSe_2:TPPO).

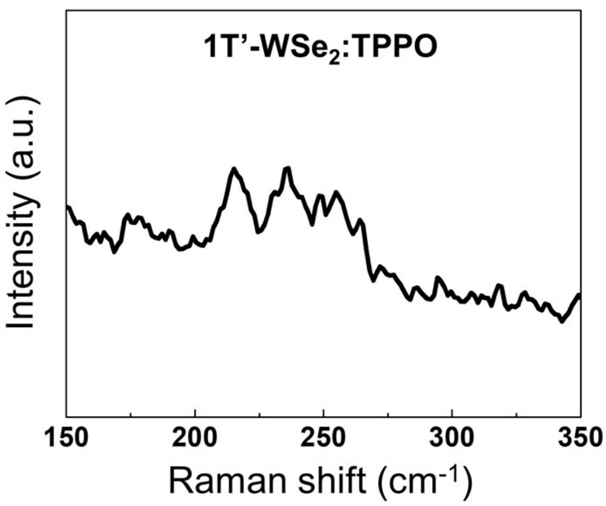

Figure S10. Raman spectrum of 1T'-WSe_2:TPPO.

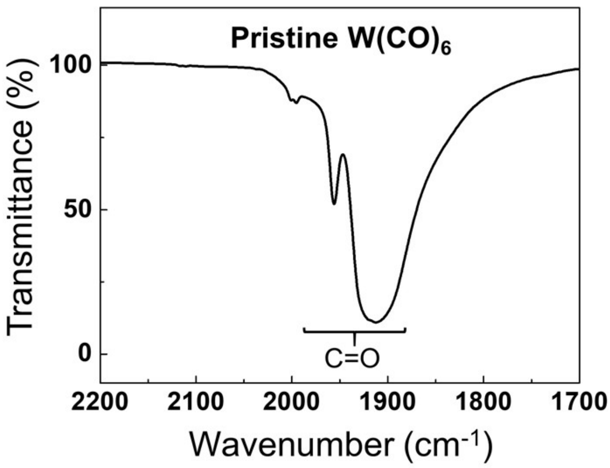

Figure S11. FTIR transmittance spectrum of pristine $W(CO)_6$, exhibiting C=O stretching signals.

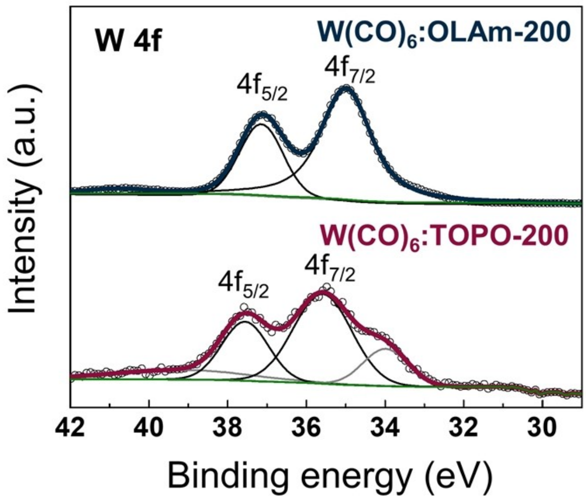

Figure S12. High-resolution W 4f XPS spectra of $W(CO)_6$:OLAm-200 and $W(CO)_6$:TOPO-200.

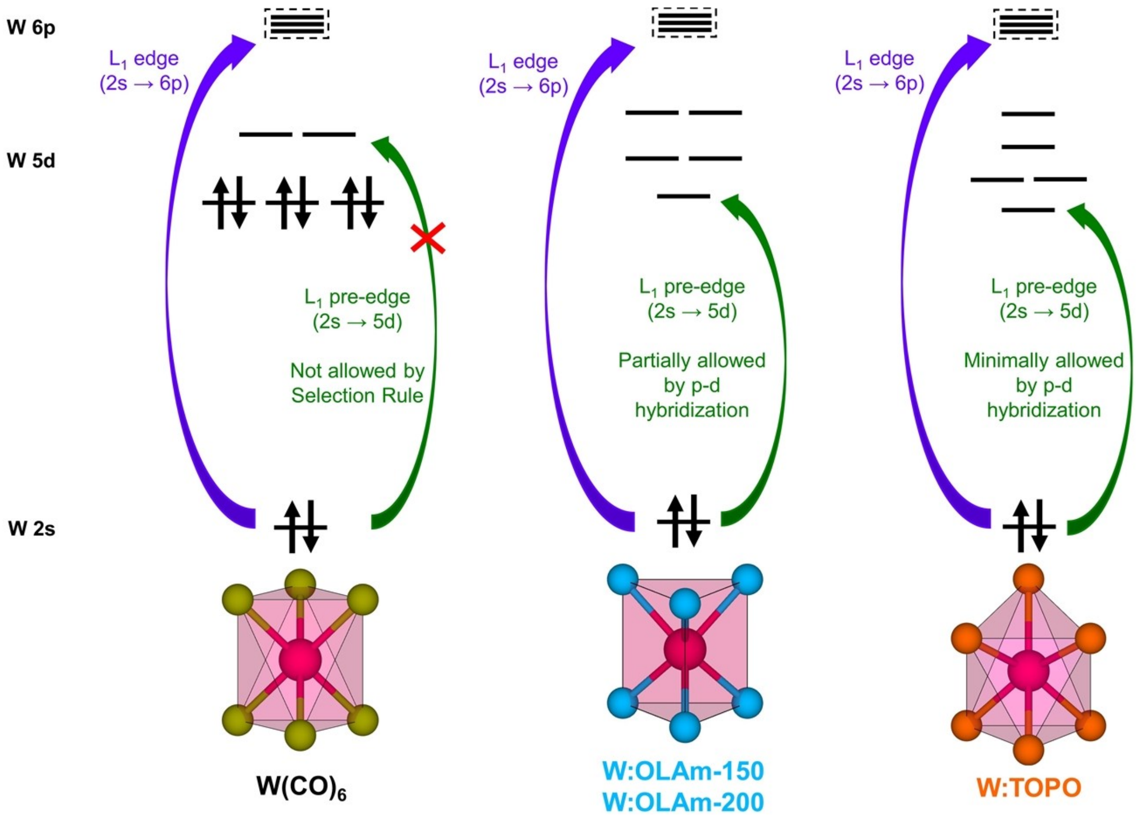

Figure S13. Schematic illustration describing a pre-edge absorption mechanism in six-coordinate W complexes.

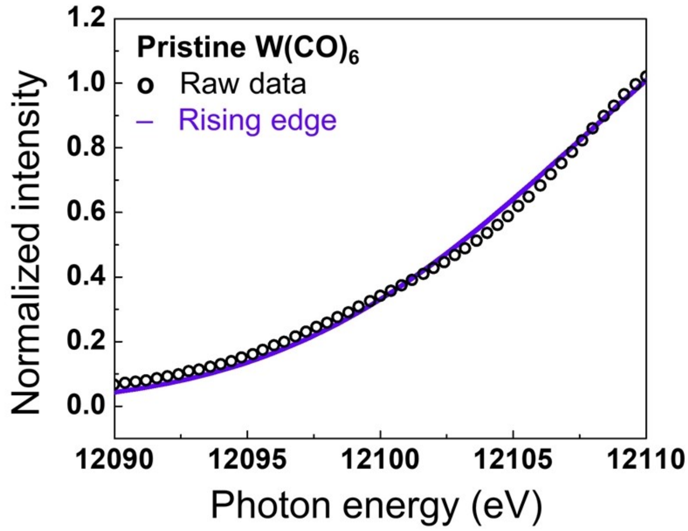

Figure S14. XANES spectrum of pristine $W(CO)_6$ at the W L_1-edge, fitted with the rising edge.

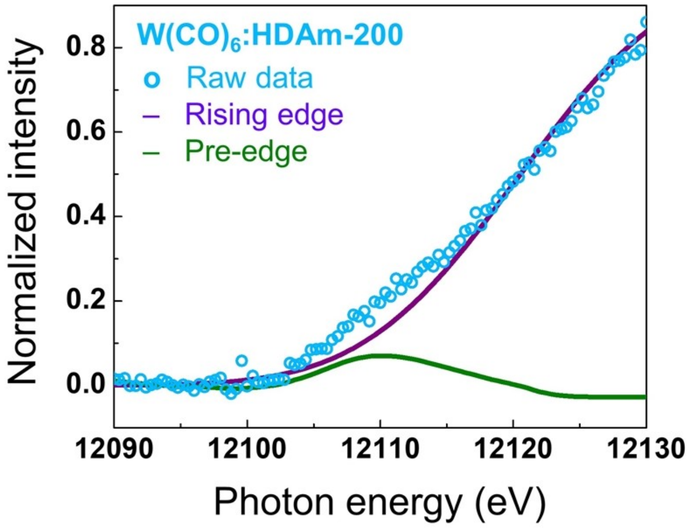

Figure S15. Fitted XANES spectrum of $W(CO)_6$:HDAm-200 at the W L_1-edge.

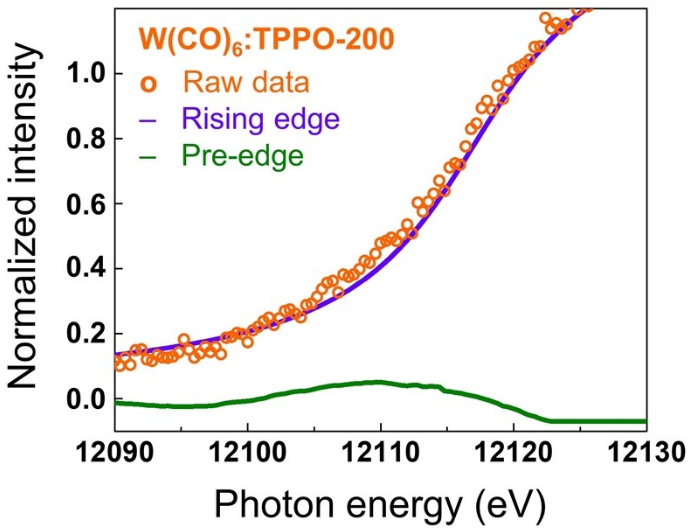

Figure S16. Fitted XANES spectrum of $W(CO)_6$:TPPO-200 at the W L_1-edge.

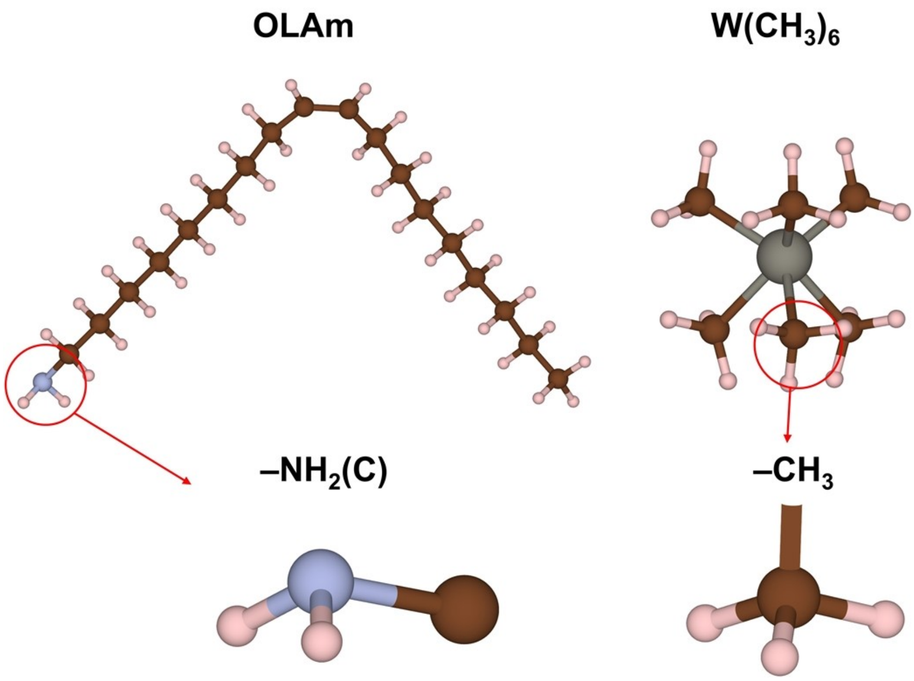

Figure S17. Tetrahedral molecular geometry of $–NH_2(C)$ in OLAm and $–CH_3$ in $W(CH_3)_6$.

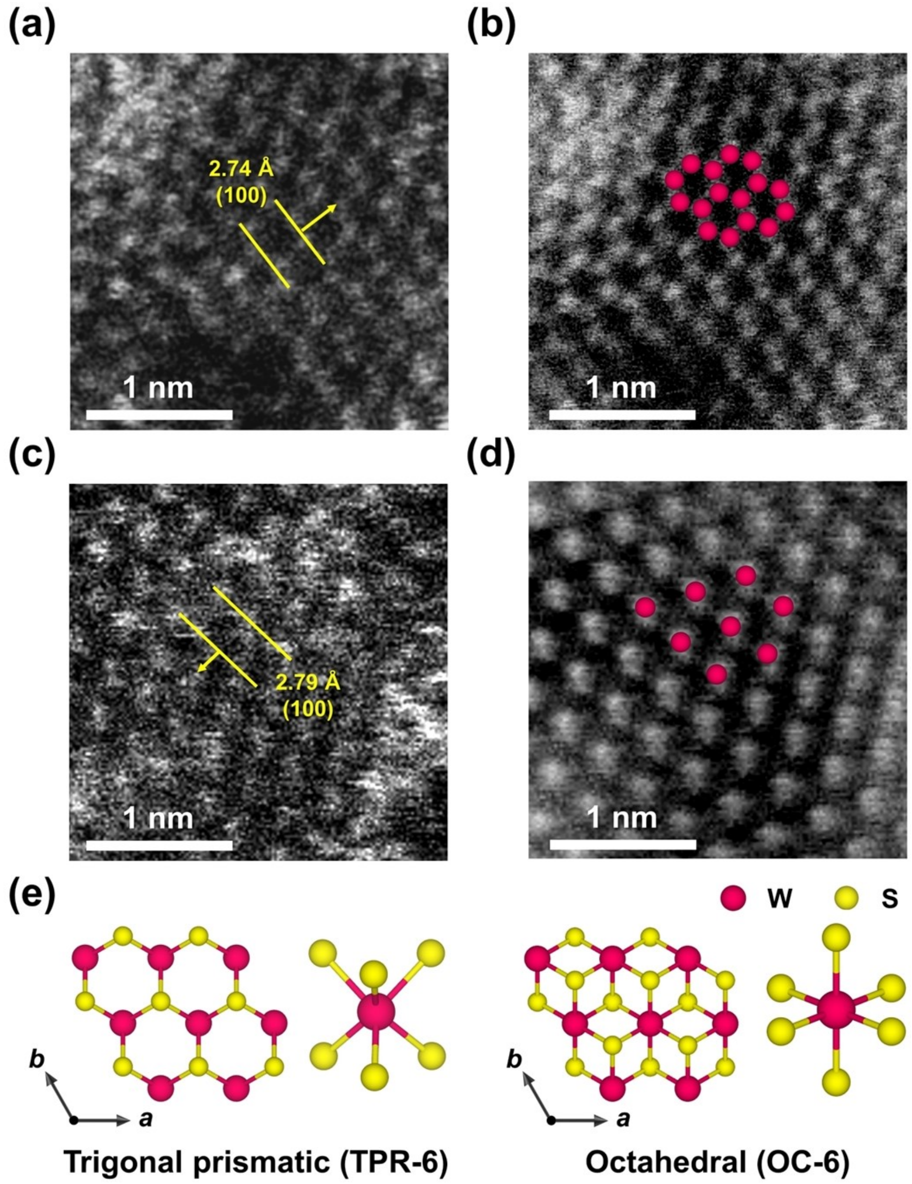

Figure S18. Top-view HAADF-STEM and inverse FFT images of (a,b) 2H-WS_2:OLAm and (c,d) 1T-WS_2:TOPO. (e) Schematic structures showing the top-view atomic arrangement and W coordination geometry in 1T-WS_2 and 2H-WS_2.

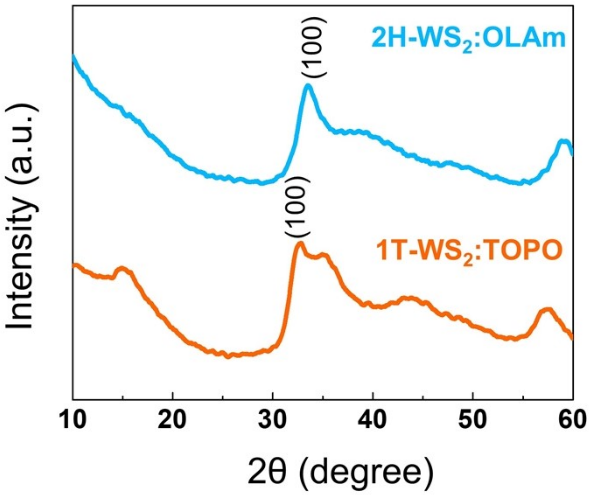

Figure S19. PXRD patterns of 2H-WS_2:OLAm and 1T-WS_2:TOPO.

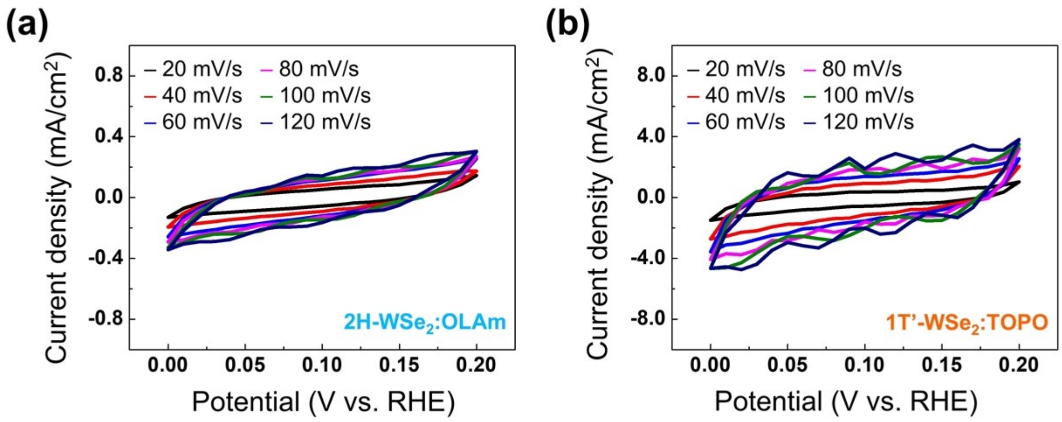

Figure S20. Cyclic voltammetry measurements of (a) 2H-WSe_2:OLAm and (b) 1T'-WSe_2:TOPO with varying scan rates.

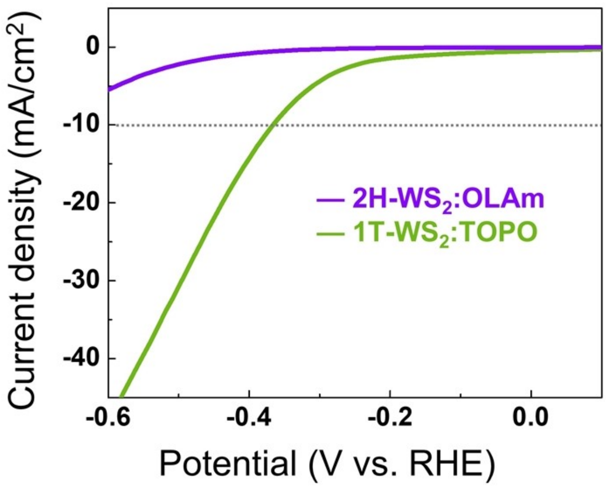

Figure S21. HER polarization curves of 2H-WS_2:OLAm and 1T-WS_2:TOPO.

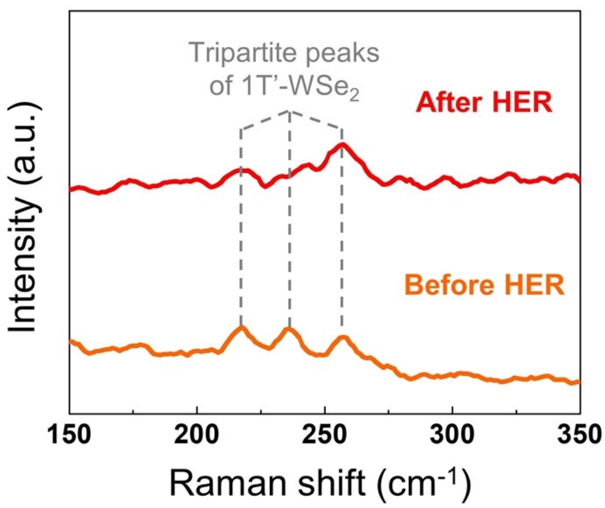

Figure S22. Raman spectrum of the 1T'-WSe_2:TOPO catalyst before and after HER long-term stability measurement.

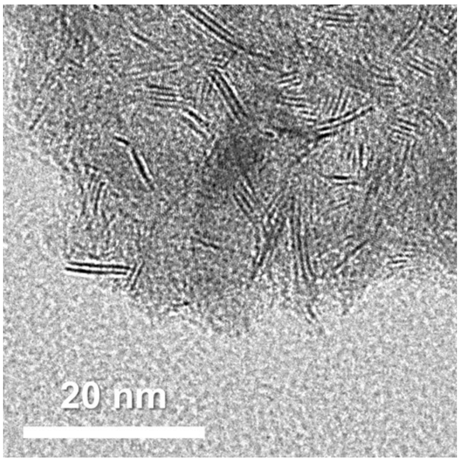

Figure S23. TEM image of the 1T'-WSe_2:TOPO catalyst after long-term stability measurement.

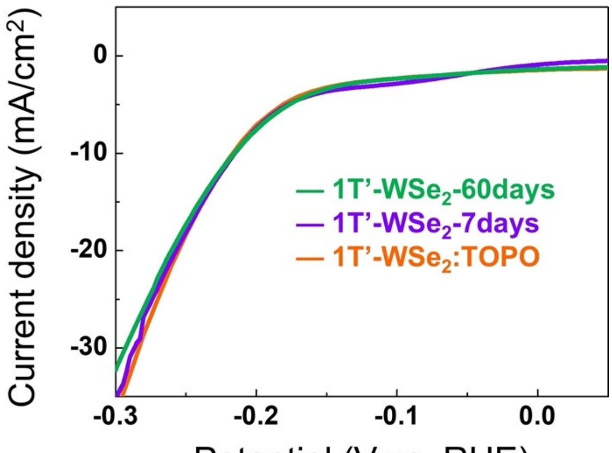

Figure S24. HER polarization curves of 1T'-WSe_2:TOPO, 1T'-WSe_2-7days, and 1T'-WSe_2-60days.

Table S2 HER performances of WCh_2 catalysts in the literatures.

Ref.	Catalyst	Overpotential (mV)	Tafel slope (mV/dec)	Stability
1	Exfoliated 1T-WS_2	250	60	120 h
2	2M phase WSe_2	104	71	120 h
3	WS2 nanoribbons	240	68	-
4	WS_2 on $W_{18}O_{49}$ nanotubes	210	122	-
5	1T-WSe_2 on substrate by heating up method	197	143	-
6	Colloidal WSe_2 nanosheets	140	101	18 h
7	$W_{0.8}Nb_{0.2}Se_2$	125	69	144 h
8	1T'-WSe_2 nano-monolayers	232	59	-
9	SLHS-1T-WS_2	153	46	36 h
	SLHS-1T-WSe_2	211	58	-
10	Colloidal 1T-WS_2	200	50	120 h
11	Layered WS_2	184	79	-
12	1T-WS_2 monolayer	185	100	-
13	WSe_2 nanostructure	259	105	3000 CV cycles
This work	1T'-WSe_2:TOPO	210	115	180 h

References

1 D. Voiry, H. Yamaguchi, J. Li, R. Silva, D. C. B. Alves, T. Fujita, M. Chen, T. Asefa, V. B. Shenoy, G. Eda and M. Chhowalla, Nat. Mater., 2013, **12**, 850-855.

2 I. S. Kwon, I. H. Kwak, J. Y. Kim, S. J. Lee, Q. A. Sial, J. Ihsan, K.-S. Lee, S. J. Yoo, J. Park and H. S. Kang, Adv. Mater., 2023, 2307867.

3 J. Lin, Z. Peng, G. Wang, D. Zakhidov, E. Larios, M. J. Yacaman and J. M. Tour, *Adv. Energy Mater.,* 2014, **4**, 1301875.

4 X. Shi, M. Fields, J. Park, J. M. McEnaney, H. Yan, Y. Zhang, C. Tsai, T. F. Jaramillo, R. Sinclair, J. K. Nørskov and X. Zheng, *Energy Environ. Sci.*, 2018, **11**, 2270-2277.

5 Y. J. Park, H. S. So, H. Hwang, D. S. Jeong, H. J. Lee, L. Lim, C. G. Kim and H. S. Shin, *ACS Nano*, 2022, **16**, 11059-11065.

6 W. Zhang, X. Liu, T. Liu, T. Chen, X. Shen, T. Ding, L. Cao, L. Wang, Q. Luo and T. Yao, *J. Phys. Chem. C*, 2021, **125**, 6229-6236.

7 I. H. Kwak, I. S. Kwon, J. Y. Kim, G. M. Zewdie, S. J. Lee, S. J. Yoo, J.-G. Kim, J. Park and H. S. Kang, *ACS Nano*, 2022, **16**, 13949-13958.

8 Z. Liu, K. Nie, X. Qu, X. Li, B. Li, Y. Yuan, S. Chong, P. Liu, Y. Li, Z. Yin and W. Huang, *J. Am. Chem. Soc.*, 2022, **144**, 4863.

9 B. Li, K. Nie, Y. Zhang, L. Yi, Y. Yuan, S. Chong, Z. Liu and W. Huang, *Adv. Mater.*, 2023, **35**, 2303285.

10 Z. Liu, N. Li, C. Su, H. Zhao, L. Xu, Z. Yin, Li. J and Y. Du, *Nano Energy*, 2018, **50**, 176-181.

11 M. M. Alsabban, S. Min, M. N. Hedhili, J. Ming, L.-J. Li and K.-W. Huang, *ECS J. Solid State Sci. Technol.*, 2016, **5**, Q3067-Q3071.

12 A. Han, X. Zhou, X. Wang, S. Liu, Q. Xiong, Q. Zhang, L. Gu, Z. Zhuang, W. Zhang, F. Li, D. Wang, L. J. Li and Y. Li, *Nat. Commun.*, 2021, **12**, 709.

13 S. R. Kadam, A. N. Enyashin, L. Houben, R. Bar-Ziv and M. Bar-Sadan, *J. Mater. Chem. A*, 2020, **8**, 1403-1416.